Clinical Cancer Research

Rebalancing Protein Homeostasis Enhances Tumor Antigen Presentation

Alex M. Jaeger[1,2], Lauren Stopfer[1,3], Sunmin Lee[4], Giorgio Gaglia[2,5], Demi Sandel[1], Sandro Santagata[5,6,7], Nancy U. Lin[8,9], Jane B. Trepel[4], Forest White[1,3], Tyler Jacks[1,10], Susan Lindquist[2,10,†], and Luke Whitesell[2]

Abstract

Purpose: Despite the accumulation of extensive genomic alterations, many cancers fail to be recognized as "foreign" and escape destruction by the host immune system. Immunotherapies designed to address this problem by directly stimulating immune effector cells have led to some remarkable clinical outcomes, but unfortunately, most cancers fail to respond, prompting the need to identify additional immunomodulatory treatment options.

Experimental Design: We elucidated the effect of a novel treatment paradigm using sustained, low-dose HSP90 inhibition *in vitro* and in syngeneic mouse models using genetic and pharmacologic tools. Profiling of treatment-associated tumor cell antigens was performed using immunoprecipitation followed by peptide mass spectrometry.

Results: We show that sustained, low-level inhibition of HSP90 both amplifies and diversifies the antigenic repertoire presented by tumor cells on MHC-I molecules through an IFNγ-independent mechanism. In stark contrast, we find that acute, high-dose exposure to HSP90 inhibitors, the only approach studied in the clinic to date, is broadly immunosuppressive in cell culture and in patients with cancer. In mice, chronic non-heat shock–inducing HSP90 inhibition slowed progression of colon cancer implants, but only in syngeneic animals with intact immune function. Addition of a single dose of nonspecific immune adjuvant to the regimen dramatically increased efficacy, curing a subset of mice receiving combination therapy.

Conclusions: These highly translatable observations support reconsideration of the most effective strategy for targeting HSP90 to treat cancers and suggest a practical approach to repurposing current orally bioavailable HSP90 inhibitors as a new immunotherapeutic strategy.

See related commentary by Srivastava and Callahan, p. 6277

Introduction

Cancers arising within diverse tissues are known to harbor numerous genetic and epigenetic aberrations that ultimately reconfigure their proteomes to support the malignant state (1). Despite the expression of hundreds to thousands of mutants, the onco-proteomes of cancers are poorly recognized by the immune system. These observations have encouraged extensive efforts to understand tumor–host immune cell interactions and how they might be manipulated for therapeutic benefit. Indeed, harnessing the power of the immune system to attack tumor cells is already revolutionizing the treatment of several types of cancer (2, 3). Most notably, therapies designed to limit T-cell exhaustion, collectively referred to as "checkpoint inhibitors," have resulted in unprecedented responses in certain patient populations with very poor prognoses (2).

Unfortunately, despite the clinical successes of checkpoint inhibitors, many patients either fail to respond, or relapse following initial response (4–6). Even cancers predicted to carry very high mutational burdens such as melanoma, smoking-associated non–small cell lung cancer (NSCLC), and microsatellite instability–high (MSI-h) tumors exhibit objective response rates to immune checkpoint–blocking antibodies of only 35%–53% (2). As an alternative, but complementary approach to harnessing the power of immune effector mechanisms, we have sought ways to increase the immunogenicity of cancer cells by unmasking their mutant proteomes.

Decades of work studying protein folding in the cell have highlighted a unique role for the molecular chaperone HSP90 in regulating the stability, function, and degradation of diverse conformationally labile proteins, including many of the mutant proteins expressed by cancers (7). More recent studies have built on this classical work to reveal a capacity for HSP90 to act as an environmentally sensitive protein-folding buffer that shapes the manifestations of genetic variation in model organisms and in man (8, 9). Critically, limiting HSP90-mediated buffering and rebalancing HSP90's chaperone function from protecting misfolding-prone mutants to presenting them for proteolytic

[1]Koch Institute for Integrative Cancer Research, Massachusetts Institute of Technology Cambridge, Massachusetts. [2]Whitehead Institute for Biomedical Research, Cambridge, Massachusetts. [3]Department of Biological Engineering, Massachusetts Institute of Technology, Cambridge, Massachusetts. [4]Developmental Therapeutics Branch, National Cancer Institute, Bethesda, Maryland. [5]Department of Pathology, Brigham and Women's Hospital, Boston, Massachusetts. [6]Ludwig Center at Harvard, Harvard Medical School, Boston, Massachusetts. [7]Laboratory for Systems Pharmacology, Harvard Medical School, Boston, Massachusetts. [8]Department of Oncologic Pathology, Harvard Medical School, Massachusetts. [9]Department of Medical Oncology, Dana Farber Cancer Institute, Boston, Massachusetts. [10]Howard Hughes Medical Institute, Chevy Chase, Maryland.

Note: Supplementary data for this article are available at Clinical Cancer Research Online (http://clincancerres.aacrjournals.org/).

†Deceased.

Corresponding Author: Luke Whitesell, University of Toronto, Toronto, Ontario M5G 1M1, Canada. Phone: 416-978-4069; Fax: 416-978-6885; E-mail: luke.whitesell@utoronto.ca

Clin Cancer Res 2019;25:6392–405

doi: 10.1158/1078-0432.CCR-19-0596

Translational Relevance

Inhibitors of the molecular chaperone HSP90 have been extensively explored as a means to treat cancer by destabilizing components of oncogenic signaling pathways. However, despite promising preclinical evidence that inhibiting HSP90 would provide better outcomes, the clinical response to these inhibitors has been disappointing and none have achieved FDA approval. Notably, unlike many other signaling inhibitors, HSP90 inhibitors have been clinically tested at intermittent, bolus dosing schedules. Here we report that such dosing results in profound immunosuppression in patients with cancer. In striking contrast, we show that sustained, low-level inhibition of HSP90 not only avoids immunosuppression associated with high doses, but also stimulates antitumor immunity by diversifying the antigenic repertoire presented on tumor cells through MHC-I. These results support reconsideration of the most effective way to use HSP90 inhibitors in the clinic and provide a blueprint to repurpose current, orally bioavailable HSP90 inhibitors as immunomodulatory treatments.

degradation can be achieved without activation of the compensatory heat shock response (HSR) driven by the transcription factor HSF1 (8, 10).

With the concept of rebalancing proteostasis as point-of-departure, we set out to destabilize the aberrant proteome of cancer cells and reveal it to host immunosurveillance mechanisms, while sparing the essential functions of HSP90 required by normal cells. We examined the effects of low-level, non-heat shock–inducing HSP90 inhibition on antigen presentation in culture and developed methods to achieve sustained, low-level HSP90 inhibition in mice. Continuous, non-heat shock–inducing HSP90 inhibition amplified and diversified the repertoire of MHC-I–associated peptides presented on tumor cells while avoiding the systemic toxicities and immunosuppression that we observed with conventional, acute high doses of HSP90 inhibitor. In combination with a nonspecific adjuvant, low-dose HSP90 inhibition translated to marked improvement in long-term survival for immunocompetent mice bearing aggressive syngeneic tumors. These observations highlight a previously unrecognized biphasic effect of HSP90 inhibition on tumor immunity and prompt reconsideration of the therapeutic goals for targeting HSP90 in cancer.

Materials and Methods

Clinical sample collection

Blood samples for gene expression analyses were obtained with informed consent from patients participating in an Institutional Review Board–approved clinical trial coordinated by the Dana-Farber Cancer Institute (Boston, MA; DFCI 11-477, NCT01560416). All samples were processed and analyzed by collaborating investigators in an anonymous fashion to preserve patient confidentiality.

NanoString analysis

Gene expression measurements using NanoString codesets were performed with NanoString XT GEx kits. Analyses were performed on total RNA from clinical samples or mouse tumor tissue following manufacturer's instructions. Briefly, 100 ng total RNA (measured by Qubit, Invitrogen), was mixed with capture and reporter probe sets and hybridized for 16–20 hours at 65°C prior to ramping down to hold at 4°C. Hybridized samples were processed on a NanoString Prep Station according to manufacturer's instructions and then scanned with an FOV setting of 1100. All files (.rcc) were analyzed using nSolver v3.0 software.

PBMC isolation and RNA sequencing

Whole blood was collected into lithium–heparin tubes and processed with Histopaque-1077 (Sigma) to isolate peripheral blood mononuclear cells as per the manufacturer's instructions. After overnight culture in RPMI1640 with 20% autologous plasma, ganetespib (500 nmol/L), fulvestrant, ganetespib + fulvestrant, or an equal volume of solvent vehicle (DMSO 0.1% v/v) was added to duplicate dishes. Incubation was continued for 24 hours after which cells were collected by centrifugation, lysed in RLT buffer (Qiagen), and total RNA isolated using an RNeasy kit as per the manufacturer's instructions (Qiagen). Sequencing library preparation was performed by the Whitehead Genome Technology Core using standard Illumina protocols and TruSeq adapters. Single-end, 40-bp sequencing was performed on a HiSeq 2000 instrument. Adapter sequences were trimmed, and reads were aligned to mm10 using TopHat2 and rpkm values generated with Cufflinks. Differential expression analysis was performed with the Bioconductor package DEseq (2).

Cell culture

MC38 cells were kindly provided by A. Sharpe from Dana Farber Cancer Institute (Boston, MA). B16-F10, H838, and SKMEL cells were obtained from ATCC, ID8 cells were obtained from Millipore Sigma, and SUM159 cells were kindly provided by N. Polyak (Dana Farber Cancer Institute). MC38 and B16-F10 cells were maintained in DMEM supplemented with 10% FBS and penicillin/streptomycin. ID8 cells were maintained in DMEM supplemented with 4% FBS, 5 μg/mL insulin, 5 μg/mL transferrin, 5 ng/mL sodium selenite, and penicillin/streptomycin. SUM159, H838, and SKMEL cells were maintained in RPMI1640 supplemented with 10% FBS and penicillin/streptomycin. Cells were confirmed negative for *Mycoplasma* contamination by PCR-based assay. For cell viability assays, 20,000 MC38 cells were seeded into 96-well plates, allowed to attach for 24 hours, and then treated with serial dilutions of Hsp90i (NVP-HSP990). Relative cell content per well was assayed after 72 hours treatment using Alamar Blue (R&D Systems) or sulforhodamine B (Sigma). For Alamar Blue assays, the stock solution was diluted 1:4 in PBS and then added directly to the 96-well plates at a 1:5 dilution (1:20 dilution final) and incubated at 37°C under 5% CO_2 for 3 hours. Fluorescence as a measure of relative dye reduction was measured on an Envision plate reader (Perkin Elmer) with excitation at 544 nm and emission readings at 570 nm.

Hsf1, Ifngr, and B2m knockout using CRISPR/Cas9

For CRISPR/Cas9–mediated gene editing, pSpCas9-P2A-GFP plasmid (Addgene #48138) was modified with a control sgRNA sequence (GTATTACTGATATTGGTGGG) or an sgRNA targeting *Hsf1* (CATGTGTCTCCTGACAGAGT), *Ifngra* (TATGTGGAGCATAACCGGAG), or *B2m* (TTGAATTTGAGGGGTTTCTG). Log-phase MC38 cells were transfected using Lipofectamine 2000 (Invitrogen) according to the manufacturer's instructions.

Twenty-four hours later, single GFP^+ cells were sorted into 96-well plates to isolate individual MC38 clones with the desired modification. For *B2m* knockout, after 2 weeks of single-cell expansion, isolated clones were tested by Western blot analysis to confirm the loss of *B2m* expression. Ctrl and B2m clones were then passaged through syngeneic mice (C57/Bl6) to increase the uniformity of tumor establishment and progression in subsequent experiments. For *Ifngra* knockout, control or sgRNA-targeting Ifngra (TATGTGGAGCATAACCGGAG) were cloned into pLenti-CRISPRv2 (Addgene #52561). Lentivirus was produced with HEK293T cells and MC38 cells were transduced with standard protocols. Transduced cells were selected with 2 μg/mL puromycin for 72 hours. Selected cells were then treated with DMSO, 60 nmol/L Hsp90i, 10 ng/mL Ifng, or the combination and analyzed by flow cytometry with anti-MHC-I antibodies (Clone AF6-88.5, BioLegend) and Ifngr antibody (GR20, BD Biosciences).

Flow cytometry

For analysis of MHC-I surface expression, cells were seeded into 12-well plates (125,000/well). Twenty-four hours later, cells were treated with the indicated concentrations of Hsp90i (NVP-HSP990), SNX-2112 (60 nmol/L), or DMSO vehicle. Seventy-two hours after the treatment, cells were dissociated with Accumax (Innovative Cell Technologies) and each treatment condition was distributed into 2 wells of a 96-well plate. Cells were spun at 500 × *g* for 3 minutes, washed 1× in ice-cold PBS supplemented with 2 mmol/L EDTA and 0.5% FBS, and incubated with PE-labeled anti-H2-K^b antibody (Clone AF6-88.5, BioLegend) or PE-labeled isotype control (Clone MOPC-173, BioLegend) at a 1:400 dilution for 45 minutes on ice. After incubation with antibody, cells were washed 1× in ice-cold PBS + 10% FBS prior to analysis on a MACSQuant VYB flow cytometer. Cytometric data were plotted and analyzed with FlowJo.

For analysis of MHC-I on MC38 tumors, mice were sacrificed by CO_2 inhalation and tumor tissue was quickly dissected and placed on ice until processing by thorough mincing with a razor and filtration through a 70-μm cell strainer. Cells were then stained with H2-K^b antibody (1:400) or isotype control as described for cultured cells.

Immunoblotting

Protein extraction was performed by washing cells two times with PBS. A volume of lysis buffer (50 mmol/L Tris pH 7.5, 150 mmol/L NaCl, 1 mmol/L EDTA, 1% Triton-X100, 0.1 % SDS, 1× Halt Protease/Phosphatase inhibitor) equal to 1/10 the culture media volume was added directly to the culture dish and incubated for 2–3 minutes on ice. Lysates were then thoroughly scraped and pipetted into 1.5-mL tubes and incubated for an additional 30 minutes on ice. Lysates were then cleared by centrifugation at 14,000 × *g* for 15 minutes and quantified using BCA Assay. Lysates were separated by SDS-PAGE and transferred to 0.2-μm nitrocellulose membranes prior to washing with PBST, blocking with 5% milk in PBST, and incubation with primary antibody overnight at 4°C. All primary antibodies were diluted 1:1,000 in 2.5% milk in PBST. Membranes were then washed 4 × 5 minutes with PBST and incubated with HRP-conjugated secondary antibody at a 1:10,000 dilution in 2.5% milk in PBST, and washed again 4 × 5 minutes with PBST. Detection of secondary antibody was performed with SuperSignal West Pico or Femto ECL reagents (Pierce) and digitally imaged on a ChemiDoc (Bio-Rad).

Mice

All experiments involving mice were performed under a protocol approved by the MIT Institutional Animal Care and Use Committee. MC38 or B16-F10 cells growing in log phase were harvested by incubation with trypsin, washed three times in PBS, and implanted (1×10^5 cells/site) into the right inguinal region of 6- to 8-week-old female (MC38) or male (B16-F10) C57Bl6 mice (Jackson Labs). Once palpable, tumors were monitored every other day via digital caliper measurements and volume calculated using the following formula: length (mm) × width (mm) × width (mm) × 520 = tumor volume in mm^3. Mice were euthanized by CO_2 inhalation, tumors were harvested and cut into thirds with a razor for histology, flow cytometry, and flash freezing in liquid N_2 for RNA/protein isolation.

For oral dosing with Hsp90i, the average water consumption of the mice was calculated by measuring water bottle weight before and after 72 hours of housing to determine the average consumption per mouse, per day. Across all experiments, C57Cl/6 mice consumed approximately 4 mL every day. Using these water consumption values, and mouse weight, a 4 mg/mL stock solution of NVP-HSP990 (in 100% PEG400) was diluted directly into the drinking water to achieve a target dose of 0.5 mg/kg/day. HSP990 treatment was begun 72 hours prior to implantation of MC38 cells to allow the drug to reach steady-state level prior to tumor challenge.

HSP990 pharmacokinetics

Serum NVP-HSP990 levels were analyzed by sacrificing mice, performing a cardiac puncture, and isolating approximately 500 μL of whole blood. Blood was transferred to EDTA-coated microtubes and placed on ice. After all samples were collected, they were spun at 10,000 × *g* for 15 minutes. The supernatant plasma was collected and stored at −80°C until further processing. A total of 2 × 10 μL aliquots of serum from each animal was extracted with 40 μL of ice-cold acetonitrile and shaken for 30 minutes at 4°C. The acetonitrile solvent was spiked with 10 nmol/L imatinib as an internal standard for mass spectrometry. Following extraction, samples were spun at 20,000 × *g* for 15 minutes and the deproteinated supernatant transferred to a clean Eppendorf tube prior to mass spectrometry analysis. Standard curves were prepared in plasma matrix at known concentrations of 0, 1.23, 3.7, 11.1, 33.3, 100, and 300 nmol/L NVP-HSP990 and processed in parallel with the experimental samples.

For mass spectrometry analysis, acetonitrile was purchased from Merck Millipore and was LC/MS Hypergrade. All other solvents were purchased from Fisher and were Optima LC/MS grade. Analysis was conducted on a QExactive benchtop orbitrap mass spectrometer equipped with an Ion Max source and a HESI II probe, which was coupled to a Dionex UltiMate 3000 UPLC system (Thermo Fisher Scientific). External mass calibration was performed using the standard calibration mixture every 7 days.

A 5-μL sample was injected onto a Kinetex 2.6 μm 50 × 2.1 mm C18 analytical column (Phenomenex). Chromatographic separation was achieved using the following conditions: buffer A was 0.1% formic acid; buffer B was 0.1% formic acid in acetonitrile. The column oven and autosampler tray were held at 35°C and 4°C, respectively. The chromatographic gradient was run at a flow rate of 0.4 mL/min as follows: 0–3.5 minutes: linear gradient 5%–80% B; 3.6–4.5 minutes: hold 98% B; 4.6–6.0 minutes: hold 5% B. The mass spectrometer was operated in positive mode using

targeted selected ion monitoring (tSIM), with the scans centered around m/z = 380.1527 (HSP990) and 494.2663 (imatinib), and an isolation window of 1.0 m/z. The resolution was set at 70,000, the AGC target at 1e5, and the maximum injection time at 150 msec. The spray voltage was set to 3.0 kV, the heated capillary held at 275°C, and the HESI probe held at 350°C. The sheath gas flow was set to 40 units, the auxiliary gas flow was set to 15 units, and the sweep gas flow was set to 1 unit. Absolute quantitation of HSP990 (using imatinib as an internal standard) was performed using an external standard curve method in Xcalibur Quanbrowser 2.2 (Thermo Fisher Scientific), the mass tolerance was set to 5 ppm.

Histology

For histologic sectioning, tumor tissue was fixed in 10% buffered formalin for 24 hours prior to transfer to 70% EtOH for storage until paraffin-embedding, sectioning, and mounting on glass slides. For CD3 and CD8 staining, slides were dewaxed, and antigen retrieval was performed in citrate buffer (10 mmol/L citric acid, pH = 6.0) and pressure-cooked. Slides were then cooled and washed in PBS + 0.1% Tween-20 (PBST). Endogenous peroxidase activity was then blocked with Dako Dual Enzyme Block (Agilent Technologies) and endogenous proteins were blocked with 2.5% goat serum in PBST. Slides were then incubated with primary anti-CD8 antibody (1:400) overnight at 4°C or anti-CD3 antibody (1:500) for 1 hour at 25°C. After incubation with primary antibody, slides were washed three times with PBST, and then incubated with HRP-conjugated secondary antibody for 30 minutes at 25°C. Slides were then washed three times with PBST prior to development with DAB substrate for 3–5 minutes until positive staining was observed.

For CD8 and CD3 quantification, slides were scanned with a Leica High Resolution slide scanner and images imported into Aperio eSlide Manager. Two independent sections from each tumor were outlined and CD3/CD8$^+$ cells were identified and quantified using the Nuclear-ID-v1 Algorithm. Individual tumor values are the average of the two tumor sections.

qRT-PCR

Total RNA isolation from cultured cells was performed after incubation in 6-well plates in the indicated conditions using RNeasy kits (Qiagen) according to the manufacturer's instructions and eluted in 50 μL MilliQ H_2O. Eluted RNA was then treated with TURBO DNase (Ambion) and quantified by Nanodrop. A total of 1.5 μg total RNA was then used for reverse transcription using the High Capacity cDNA Reverse Transcription Kit (Applied Biosystems) with random hexamers as primers. cDNA was then diluted 1:10 prior to PCR amplification with PowerUp SYBR Green Master Mix (Applied BioSystems) in a QuantStudio6 Real Time PCR System (Applied Biosystems) according to manufacturer's instructions. C_t values were normalized to Rpl19 or Gapdh as housekeeping control and fold changes calculated with the DMSO sample as reference.

For analysis of tissues, samples (2–3 mm^3) were homogenized in 1 mL of Trizol (Molecular Research Center), phase separated with 200 μL chloroform, and precipitated with 100% isopropanol prior to resuspension in MilliQ H_2O and quantification with Nanodrop. RNA was then processed as described above for qRT-PCR.

MHC-I peptide profiling

MC38 cells were cultured as described above. 10–10 cm (~1 × 10^8 cells) plates of MC38 cells were cultured for 72 hours in 0.1% DMSO or 50 nmol/L HSP990. At the time of harvest, plates were washed 1× in PBS, and then cells were lifted using PBS + 2 mmol/L EDTA. Cells were then pelleted at 500 × *g* for 5 minutes and the pellets washed twice more with ice-cold PBS. Pellets were then resuspended in 1 mL IP lysis buffer [20 nmol/L Tris pH 7.5, 150 mmol/L NaCl, 1% CHAPS, 0.2 mmol/L PMSF, 1× HALT protease/phosphatase inhibitors (Pierce)]. Lysates were then sonicated with a microtip sonicator for 3 × 10-second pulses to further disrupt cell membranes, and then centrifuged at 14,000 × *g* for 10 minutes. The supernatant was then quantified and 10 mg total protein lysate was used for the MHC-I IP.

Peptide MHC isolation was performed using a modified immunoprecipitation and protein filtration protocol, as described previously. Briefly, for each sample, 250 μg of anti-H2-K^b clone (Y3, BioXCell) and 250 μg anti-H2^{Db} (clone B22-249, Thermo Fisher Scientific) were bound to 20 μL (bed volume) FastFlow Protein A Sepharose beads (GE Healthcare) by incubating for 3 hours at 4°C. Beads were then washed with lysis buffer and 10 mg of lysate was added and incubated overnight rotating at 4°C. Beads were then centrifuged at 2,000 rpm, washed twice with 1× TBS, and eluted with 10% acetic acid at room temperature. Eluate was then filtered using 10 kDa MWCO spin filters (PALL Life Science), which were passivated according to manufacturer's instructions and acidified prior to filtration. Isolated peptides were concentrated with vacuum centrifugation and stored at −80°C until LC/MS-MS analysis.

Mass spectrometry analysis of MHC peptides

For mass spectrometry analysis, peptides were resuspended in 0.1% acetic acid and loaded on a precolumn packed in house [100 μm ID × 10 cm packed with 10 μm C18 beads (YMC gel, ODS-A, 12 nm, S-10 μm, AA12S11)]. The precolumn was then washed with 0.1% acetic acid and connected in series to an analytical capillary column with an integrated electrospray tip (~1 μm orifice) with 5 μmol/L C18 beads, prepared in house [50 μm ID × 12 cm with 5 μm C18 beads (YMC gel, ODS-AQ, 12 nm, S-5 μm, AQ12S05)].

Peptides were eluted using a 130-minute gradient with 10%–45% buffer B (70% acetonitrile, 0.2 mol/L acetic acid) from 5 to 100 minutes and 45%–55% from 100 to 120 minutes at a flow rate of 0.2 mL/minute for a flow split of approximately 10,000:1. Peptides were analyzed using a Thermo Q Exactive HF-X Hybrid Quadrupole-Orbitrap mass spectrometer. Standard mass spectrometry parameters were as follows: spray voltage, 2.5 kV; no sheath or auxiliary gas flow; heated capillary temperature, 250°C. The HF-X was operated in data-dependent acquisition mode. Full-scan mass spectrometry spectra [mass/charge ratio (m/z), 350 to 2,000; resolution, 60,000] were detected in the Orbitrap analyzer after accumulation of ions at 3e6 target value. For every full scan, the 15 most intense ions were isolated (isolation width of 0.4 m/z) and fragmented [collision energy (CE): 28%] by higher energy collisional dissociation (HCD) with a maximum injection time of 350 milliseconds and 30,000 resolution. Dynamic exclusion was set to 15 seconds.

Mass spectrometry data analysis

Raw mass spectral data files were analyzed with Proteome Discoverer version 2.2 (Thermo Fisher Scientific) and searched

against the mouse SwissProt database and mutant peptide MC38 database using Mascot version 2.4 (Matrix Science). Spectra were matched with a mass tolerance of 10 ppm for precursor masses and 20 mmu for fragment ions. Peptides were filtered according to an ion score $\geq$16, isolation interference $\leq$30%, rank 1, and between 7 and 15 amino acids in length. Raw files were then subjected to label-free quantification in Proteome Discoverer with area as the quantification metric. Peptides that received quantification values in at least two matched replicate samples were used and the fold change of treated over DMSO control was averaged across replicates.

Statistical analysis and graphics

All graphical representations of data were generated in GraphPad Prism 7 or Adobe Illustrator with the exception of Supplementary Fig. S1C, which was generated in RStudio. NanoString data analysis was performed using nSolver 3.0 software and the Advanced Analysis module for PanCancer Immune Profiling. Differential expression analysis of RNAseq data was performed with the Bioconductor package DEseq[2]. For tumor growth curves, statistical analysis was performed with three-way ANOVA followed by Tukey multiple comparison's test. Tumor mass comparisons were made with two-way ANOVA followed by Tukey multiple comparison's test. MHC-I staining of dissociated tumor cells was performed with two-tailed, unpaired, Welch *t* test. For qPCR and FACS analysis comparisons, two-way ANOVA followed by Tukey multiple comparison test was performed. Right-censored Kaplan–Meier analysis was used for the survival curves in Fig. 4C (*, $P < 0.05$; **, $P < 0.01$; ***, $P < 0.001$; ****, $P < 0.0001$; ns, not significant).

Data accessibility

RNA-sequencing data have been deposited into the NCBI Gene Expression Omnibus (GSE113465). The mass spectrometry proteomics data have been deposited to the ProteomeXchange Consortium via the PRIDE partner repository with the dataset identifier PXD009542 and 10.6019/PXD009542.

Results

Clinically recommended doses of HSP90 inhibitor are immunosuppressive

The immunologic consequences of current clinical strategies targeting HSP90 function are not well understood. To examine the impact of HSP90 compromise on the immune system in human patients with cancer receiving the recommended dosing of an HSP90 inhibitor, we profiled the RNA expression of immune-related genes in whole blood collected from 20 patients with metastatic estrogen receptor–positive breast cancer. Patients were enrolled in a phase II study comparing the therapeutic efficacy of the pure anti-estrogen fulvestrant as a single agent or in combination with the potent and selective HSP90 inhibitor ganetespib (NCT01560416).

We obtained samples from ganetespib-treated patients at three time-points: prior to HSP90 inhibitor dosing (baseline), at 4 hours and at 20–24 hours post-intravenous administration of a conventional heat shock–inducing dose of HSP90 inhibitor (Fig. 1A). We used nCounter PanCancer Immune Profiling Panels (XT-CSO-HIP1-12, NanoString Technologies Inc.) to simultaneously measure the expression of 730 immune-related genes and 40 reference genes.

Strikingly, in these clinical samples, we found broad downregulation of diverse immune-related genes 20–24 hours after ganetespib administration (Fig. 1B). Among the most greatly affected genes were those involved in antigen presentation, a critical component of adaptive immunity and immunosurveillance of tumors (11, 12). Genes involved in antigen production via the immunoproteasome (PSMB8, PSMB9), antigen import into the endoplasmic reticulum (TAP1 and TAP2), and genes involved in surface presentation of antigen (HLA-A, HLA-E) were collectively downregulated following treatment (Fig. 1B). These observations corroborate previous reports in model systems demonstrating decreased antigen presentation following acute HSP90 inhibition, which leads to decreased T-cell–mediated killing (13).

We also found that administration of ganetespib at its recommended phase II dose resulted in downregulation of precurated gene sets assembled to survey additional immune-related functions (Fig. 1C; Supplementary Fig. S1A; ref. 14). As an internal control, we also confirmed activation of the classical heat shock response by HSP90 inhibitor at 4 hours post drug administration, which returned to baseline at 24 hours, suggesting that broad immunosuppression is a downstream consequence of heat shock–inducing exposure to HSP90 inhibitor (Supplementary Fig. S1B).

To further evaluate the immunosuppressive effect of high-level HSP90 inhibition, we cultured freshly isolated human peripheral blood mononuclear cells (PBMC) in ganetespib (500 nmol/L for 20 hours) and measured the effects on RNA expression genome-wide (Fig. 1D; Supplementary Fig. S1C). HSP90 inhibition significantly altered the gene expression profile of these cells, and Gene Ontology (GO) analysis revealed that the most upregulated functional categories of genes were related to protein folding and molecular chaperone function, whereas the most downregulated categories were immune-related pathways (Fig. 1D and E). Notably, when PBMCs were treated with fulvestrant alone, little to no changes in gene expression were observed strongly suggesting that the immunosuppressive effects observed in patients following ganetespib treatment are driven through acute HSP90 inhibition (Supplementary Fig. S1C–S1F). Taken together with previous reports in preclinical models showing that acute, high-dose HSP90 inhibition exerts immunosuppressive activities, these data indicate that current strategies for HSP90 inhibition in clinical trials suppress innate and adaptive immune function and may compromise antitumor immune responses (13, 15–19).

Continuous low-dose HSP90 inhibition stimulates antitumor immune responses

The reservoir of HSP90 in cells is significantly higher than that needed to maintain essential HSP90-dependent functions under basal conditions (20). However, excess HSP90 is important for maintaining integrity of the cellular proteome in response to challenges such as hyperthermia, hypoxia, reactive oxygen species, and conformation-destabilizing mutations and polymorphisms (9, 21). This role has given rise to the concept of HSP90 serving as a protein-folding "buffer," and recent evidence suggests that limiting this buffer can have profound phenotypic consequences in diverse organisms without acute toxicity (8, 22, 23). As the aberrant proteomes of many cancers depend on HSP90 buffering capacity, we posited that continuous, low-dose administration of an HSP90 inhibitor would alter the intracellular fate of

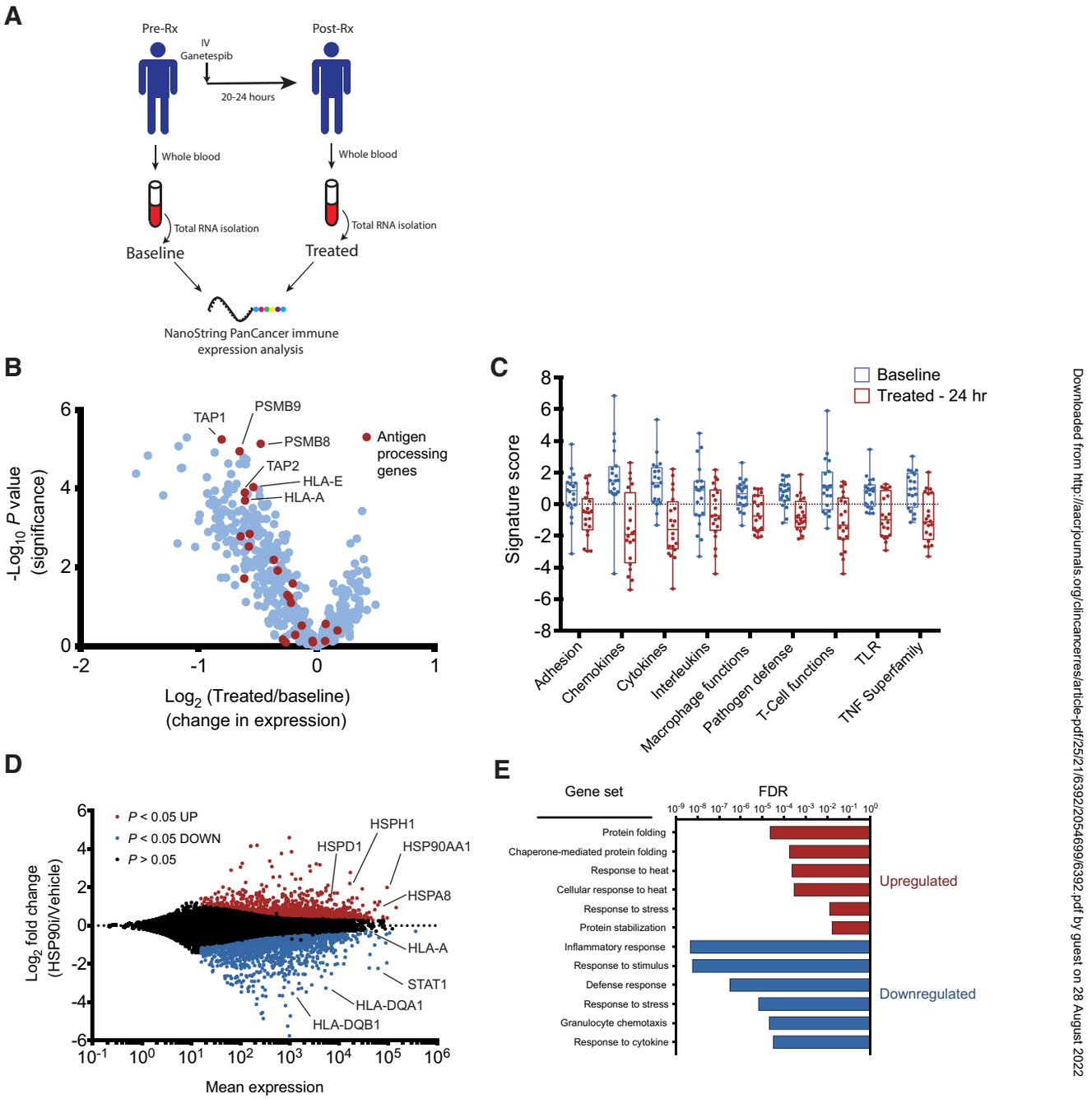

Figure 1.

Clinically recommended doses of HSP90 inhibitors are immunosuppressive. **A,** Schematic representation of the sample collection process. Whole blood was collected at baseline and 20–24 hours post intravenous (IV) HSP90 inhibitor (ganetespib) prior to total RNA isolation and analysis by NanoString Expression Profiling. **B,** Volcano plot of 521 immune-related genes passing Nanostring quality control metrics. Genes functionally related to antigen processing are highlighted in red and the top six most significantly downregulated antigen-processing genes are indicated. **C,** Immune Pathway scoring of gene expression data using NanoString Advanced Analysis. Signature scores are generated from a principal component analysis of gene-sets related to each immune pathway. Each point represents an individual patient. All 9 pathways shown are significantly downregulated following treatment (adjusted $P < 0.05$). **D,** Plot of the log ratio versus mean expression (MA plot) of transcripts analyzed by RNA-seq of human PBMCs treated with DMSO vehicle or ganetespib for 20 hours. Red points represent genes that are significantly upregulated and blue points represent significantly downregulated genes (DEseq[2] adjusted P value < 0.05). **E,** Gene ontology analysis of RNA-seq data using Panther (pantherdb.org). The top six enriched gene sets [ranked by False Discovery Rate (FDR)] for significantly upregulated (red) and downregulated (blue) genes following ganetespib treatment.

both "passenger" and "driver" mutants and hence the malignant potential of cells expressing them without incurring the undesirable immunosuppressive effects of high-dose, heat shock–inducing HSP90 inhibitor exposures (10).

To test this hypothesis, we developed a procedure to maintain continuous low nanomolar plasma concentrations of an orally bioavailable HSP90 inhibitor (NVP-HSP990; herein referred to as Hsp90i) in mice by administering it in their drinking water and a robust bioanalytical method to measure its concentration in plasma (Supplementary Fig. S2A and S2B). Recognizing the potential importance of effects on immune surveillance, we compared the effect of continuous low-dose treatment with Hsp90i on the growth of transplanted mouse MC38 colon adenocarcinoma tumors in syngeneic (C57Bl/6) and immunocompromised (NOD-SCID) hosts.

In syngeneic hosts, continuous low-dose administration of Hsp90i exerted a marked effect in MC38 tumors with a greater than 50% reduction in both tumor volume and tumor mass 18 days postimplantation (Fig. 2A and B). The efficacy we observed is equal to or greater than that observed in other reports using intermittent, high doses of HSP90 inhibitor in this model (24, 25). We also found that low-dose Hsp90i administration

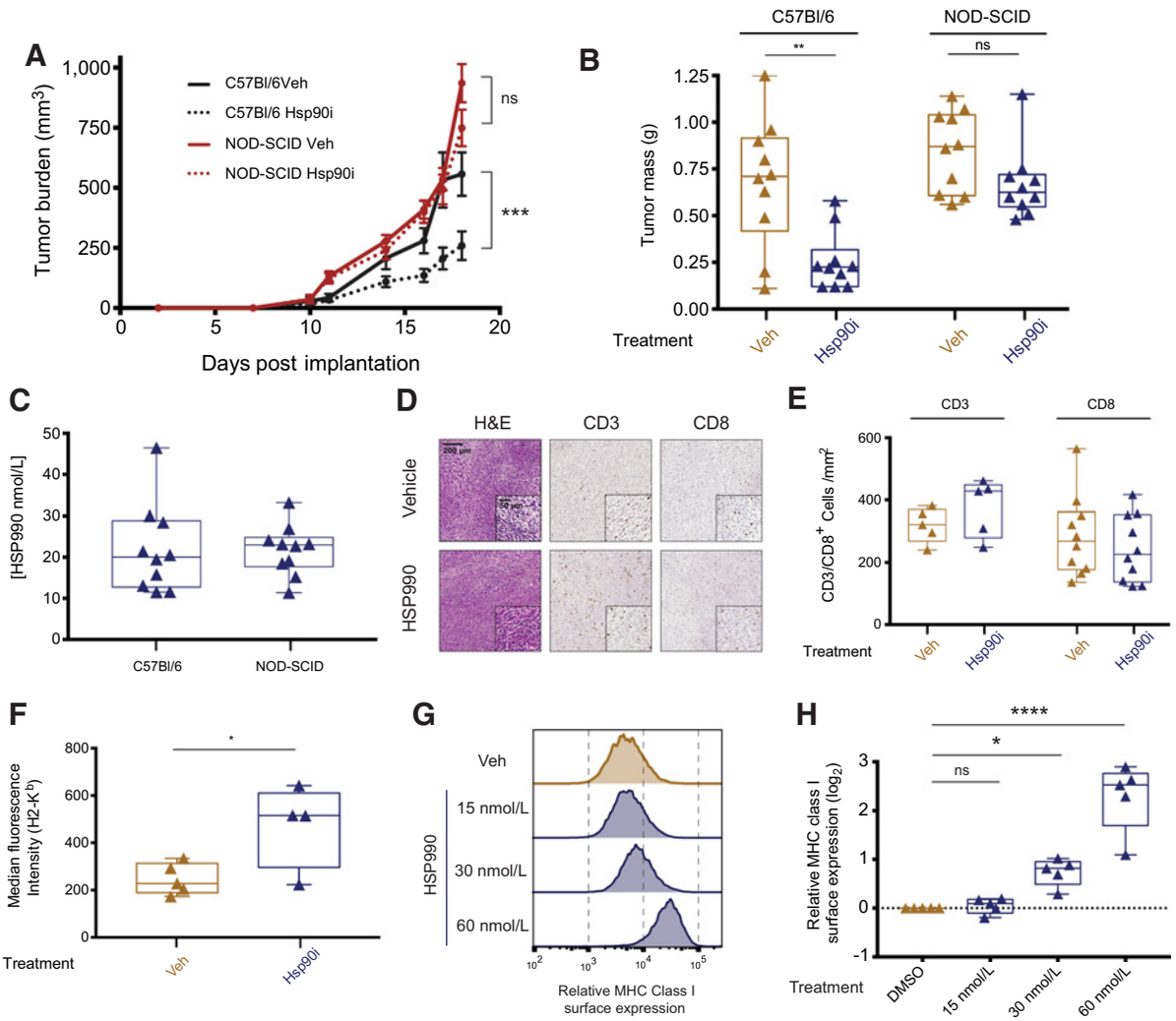

Figure 2.

Continuous low-dose HSP90i treatment reduces tumor burden in a syngeneic mouse model of colon cancer. **A,** Subcutaneous MC38 tumor growth in C57Bl/6 (black lines) or NOD-SCID (red lines) mice were treated via drinking water with vehicle (solid lines) or 0.5 mg/kg/day Hsp90i (dotted lines; $n = 10$ per group). ***, $P < 0.001$, three-way ANOVA, Tukey multiple comparison test. **B,** MC38 tumor weights in C57Bl/6 or NOD-SCID mice 18 days postimplantation. **, $P < 0.01$, two-way ANOVA, Tukey multiple comparison test. **C,** Plasma concentration of Hsp90i in Bl/6 and NOD-SCID mice measured by quantitative liquid chromatography/mass spectrometry assay ($n = 10$ per group). **D,** Representative H&E, CD3, and CD8 staining of MC38 tumors from mice treated with vehicle or Hsp90i. Large images are at 4× magnification and inset are 20×. **E,** Image quantification of the abundance of $CD3^+$ ($n = 5$) or $CD8^+$ ($n = 10$) cells per tumor area in vehicle or Hsp90i-treated mice. **F,** Flow cytometric analysis of MHC-I H2-K^b surface expression on dissociated MC38 tumor cells. ($n = 5$ for Veh, $n = 4$ for Hsp90i) *, $P < 0.05$ two-tailed, unpaired, Welch t test. **G,** Representative flow cytometric histograms of MC38 cells treated *in vitro* with the indicated Hsp90i concentrations and stained to detect MHC-I H2-K^b cell surface expression. **H,** Quantification of five independent biological replicates of samples (*, $P < 0.05$; ****, $P < 0.0001$).

reduces tumor burden in the MC38 and B16-F10 melanoma model even with delayed administration of low-dose Hsp90i (Supplementary Fig. S2C and S2D). Even more interestingly, such Hsp90i exposure had no effect on MC38 tumor growth in NOD-SCID mice, which lack normal T- and B-cell function leading to profoundly impaired adaptive immune function (Fig. 2A and B). This outcome suggests that continuous low-dose exposure to Hsp90i elicited an antitumor immune response sufficient to impede the progression of these very aggressive transplantable rodent tumors. Critically, the difference in Hsp90i efficacy between C57Bl/6 and NOD-SCID mice could not be explained by differences in drug exposure because nearly identical plasma concentrations of Hsp90i (~20 nmol/L) were present in both strains of mice (Fig. 2C; Supplementary Fig. S2B).

To investigate the mechanism(s) underlying the difference in the antitumor response of low-dose Hsp90 inhibition between immunocompetent and immunosuppressed mice, we first characterized the immune infiltrate present in tumors from control and drug-treated mice. Surprisingly, no significant difference was observed in the total number of $CD3^+$ or $CD8^+$ T cells in the tumors as measured by IHC, which suggests that the effect of Hsp90i is not mediated through T-cell recruitment (Fig. 2D and E). A recent report demonstrated that the abundance of infiltrating $CD8^+$ T cells within the tumor is not predictive of a productive immune response, but rather the compatibility of the infiltrating T-cell receptor (TCR) repertoire and available tumor antigens is the main driver of antitumor immunity (26). These observations raise the possibility that the Hsp90i-mediated response is primarily driven through diversifying the available antigens within the tumor.

Given our expression profiling results demonstrating that high-level Hsp90i impairs antigen presentation in clinical samples and *ex vivo*–treated human lymphocytes, we next assessed the expression of MHC-I on dissociated tumor cells. Intriguingly, we found higher levels of MHC-I surface expression on dissociated MC38 tumor cells isolated from Hsp90i-treated mice (Fig. 2F). We also observed that Hsp90i stimulated MHC-I surface expression on cultured MC38 cells at concentrations well below the IC_{50} for cytotoxicity (Fig. 2G and H; Supplementary Fig. S2E). These results suggest that rather than impairing immune responses, low-dose Hsp90i can actually stimulate antigen presentation on tumor cells and lead to more robust tumor recognition by immune cells. Supporting this hypothesis, NanoString expression analysis of MC38 tumor tissue revealed that low-dose Hsp90i exposure did not result in broad downregulation in immune gene expression as observed in clinical samples, and reassuringly, we also found no evidence of HSR activation by our continuous low-dose Hsp90i administration protocol (Supplementary Fig. S2F–S2H). In addition, Hsp90i stimulated MHC-I expression on mouse cell lines derived from colon, ovarian, and melanocytic malignancies and on human tumor cell lines originating from breast, melanocytes, and lung, suggesting that this strategy may be broadly applicable (Supplementary Fig. S2I).

Hsp90i stimulates MHC-I antigen presentation independent of IFNγ signaling

To better understand the mechanism(s) by which Hsp90i stimulates a more effective antitumor immune response to MC38 cells, we turned to experiments in cell culture. First, we confirmed that a chemically distinct, orally bioavailable HSP90 inhibitor, SNX-2112, caused similar induction of MHC-I surface expression (Supplementary Fig. S3A). Next, to ascertain whether Hsp90i induction of MHC-I is dependent on the HSR, we used CRISPR/Cas9 in MC38 cells to knock out Hsf1, the primary transcriptional regulator of the HSR. Importantly, low-level Hsp90i stimulated MHC-I surface expression even in the absence of Hsf1 (Supplementary Fig. S3B and S3C). Seeking to explore alternative mechanisms and given the central role of the immunoproteasome (IP) in antigen presentation (27), we examined the protein levels of Psmb8, the primary catalytic subunit of IPs. Notably, low-dose Hsp90i increased the protein levels of Psmb8, and slightly decreased the constitutive 20S proteasomal subunit Psmb5 at 72 hours (Fig. 3A), indicating a shift in the proteolytic repertoire of cells treated with Hsp90i. This effect was not observed at 24 hours postinitiation of Hsp90i, even at high concentrations, further supporting the conclusion that induction of Psmb8 is not through the classical HSR (Fig. 3A). The importance of the IP in increasing MHC-I expression in response to Hsp90i is reinforced by the observation that the expression of genes encoding immunoproteasome subunits is increased following Hsp90i (Fig. 3C; Supplementary Fig. S3D and S3E), and by the observation that a Psmb8-specific inhibitor (ONX-0914; ref. 28) abrogated increases in MHC-I surface expression caused by low-level Hsp90i treatment (Fig. 3B; Supplementary Fig. S3E).

Canonically, MHC-I expression is stimulated by exposure to the cytokine IFNγ, which is secreted by diverse infiltrating immune cells (29). IFNγ binding to the IFNγ-receptor (Ifngr) initiates a signaling cascade through the kinases JAK1/2 and the transcription factors STAT1/3 to induce the expression of diverse genes involved in antigen processing and presentation, as well as genes encoding the heavy and light chain of MHC-I. Importantly, IFNγ also results in the expression of the immunosuppressive marker PD-L1 on the surface of tumor cells which serves as a ligand for the PD-1 receptor on T cells to attenuate antitumor immune responses (30, 31). In contrast to canonical IFNγ-stimulated antigen presentation, exposure to Hsp90i did not alter transcript levels of MHC-I heavy chains *H2-K1* and *H2-D1* or the light chain beta-2-microglobulin (*B2m*), indicating that Hsp90i induces antigen presentation through a distinct mechanism (Fig. 3C). However, both Hsp90i and IFNγ stimulated expression of genes involved in antigen processing including Psmb8, Tap2, and Tapbp. Remarkably, while IFNγ robustly induced the expression of PD-L1 at the transcript, protein, and surface expression level, Hsp90i did not, suggesting that Hsp90i induces antigen presentation without driving PD-L1–mediated immunosuppression (Fig. 3C–E). Also, IFNγ, but not Hsp90i, activates Stat1 expression and phosphorylation (Fig. 3C and D). Notably, both Hsp90i and IFNγ stimulated the expression of the immunosuppressive enzyme Ido1, potentially highlighting a novel combination therapy strategy for Hsp90i, as Ido1 inhibitors have been explored in the clinic (ref. 32; Fig. 3C). Collectively, these results demonstrate that Hsp90i engages transcriptional and posttranslational mechanisms to upregulate surface MHC-I that are distinct from IFNγ signaling.

Decreased MHC-I antigen presentation through downregulation or mutation in the IFNγ signaling pathway has been identified as a clinically relevant mechanism of resistance to checkpoint blockade (33–35). On the basis of our findings, we asked

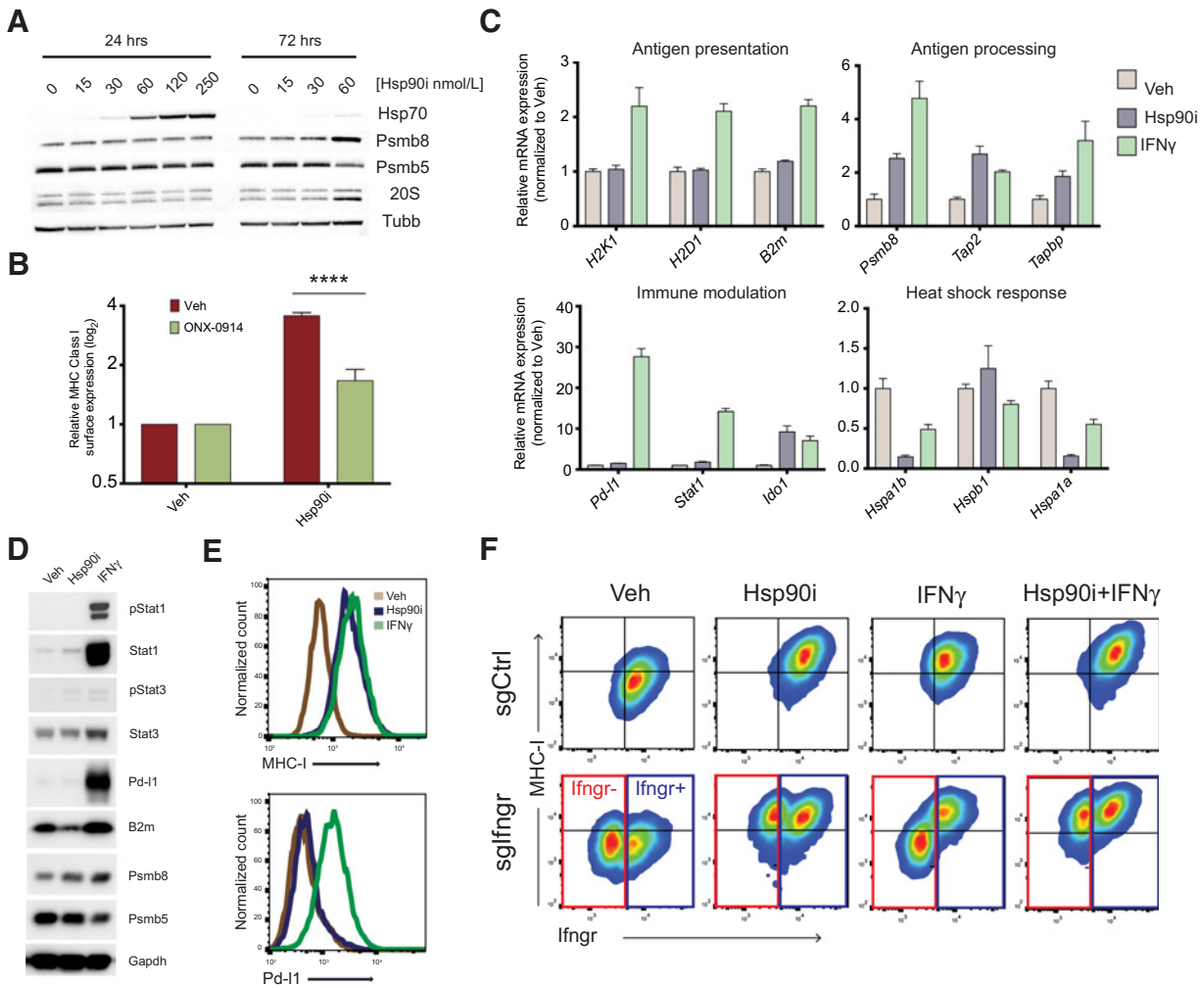

Figure 3.

Low-level Hsp90i stimulates MHC-I expression in a non-IFNγ–dependent manner. **A,** Immunoblot of HSR marker (Hsp70), immunoproteasome subunit (Psmb8), constitutive proteasome subunit (Psmb5), total proteasome (20S), and loading control (Tubb) in MC38 cells treated with Hsp90i for 24 or 72 hours at the indicated doses. **B,** Cell surface expression of MHC-I on MC38 cells treated with vehicle or Hsp90i in combination with DMSO or ONX-0914 (500 nmol/L). Normalized values calculated on the basis of the median fluorescence intensity of the baseline sample for DMSO- or ONX-0914–treated samples ($n = 3$). **C,** qRT-PCR analysis of antigen processing and presentation genes, immune checkpoint genes, and heat shock–inducible genes following 72-hour treatment with Hsp90i (60 nmol/L) or IFNγ (10 ng/mL). All treated samples were normalized to DMSO = 1 ($n = 3$). **D,** Immunoblot analysis of downstream markers of IFNγ signaling in MC38 cells following 72-hour treatment with Hsp90i (60 nmol/L) or IFNγ (10 ng/mL). **E,** Representative flow cytometric histograms of MHC-I and PD-L1 on MC38 cells treated with vehicle control (tan), Hsp90i (blue), or IFNγ (green). **F,** MHC-I expression on MC38 cells infected with Cas9 and either control short guide RNA (sgCtrl) or short guide RNA targeting the alpha chain of the IFNγ receptor (sgIfngr). Two-dimensional flow cytometric plots depict intensity of MHC-I staining (*y*-axis) and Ifngr staining (*x*-axis) following treatment with Veh, Hsp90i, IFNγ, or Hsp90i + IFNγ. Cells lacking the Ifngr are highlighted in the red box, whereas Ifngr$^+$ cells are depicted in the blue box.

whether Hsp90i mediated MHC-I presentation could rescue antigen presentation and bypass the requirement for IFNγ signaling. To examine this possibility, we infected MC38 cells with lentivirus encoding Cas9 and a control sgRNA (sgCtrl) or an sgRNA against the alpha chain of the IFNγ receptor (sgIfngr). In the sgCtrl-infected cells, Hsp90i, IFNγ, and the Hsp90i+IFNγ combination robustly induced MHC-I expression (Fig. 3F). As expected for a nonclonally selected pool of cells targeted with the sgIfngr, we observed both Ifngr− (red) and Ifngr+ (blue) cell populations, resulting in an internally controlled experimental system (Fig. 3F). In this system, IFNγ increases MHC-I levels in Ifngr+ cells, but fails to induce MHC-I expression in the Ifngr− cells. In contrast, Hsp90i is able to induce MHC-I independent of Ifngr expression (Fig. 3F).

Hsp90i amplifies and diversifies the antigen repertoire presented by MHC-I

MHC-I peptide profiling has emerged as a powerful tool to study the antigen repertoire presented by tumor cells (36). To learn whether Hsp90i and IFNγ altered the antigenic profile of MC38 cells, we performed MHC-I immunoprecipitation followed by peptide mass spectrometry of isolated antigens (depicted schematically in Fig. 4A; ref. 37). The peptides we identified in all samples were enriched for peptides of the expected size (8–11

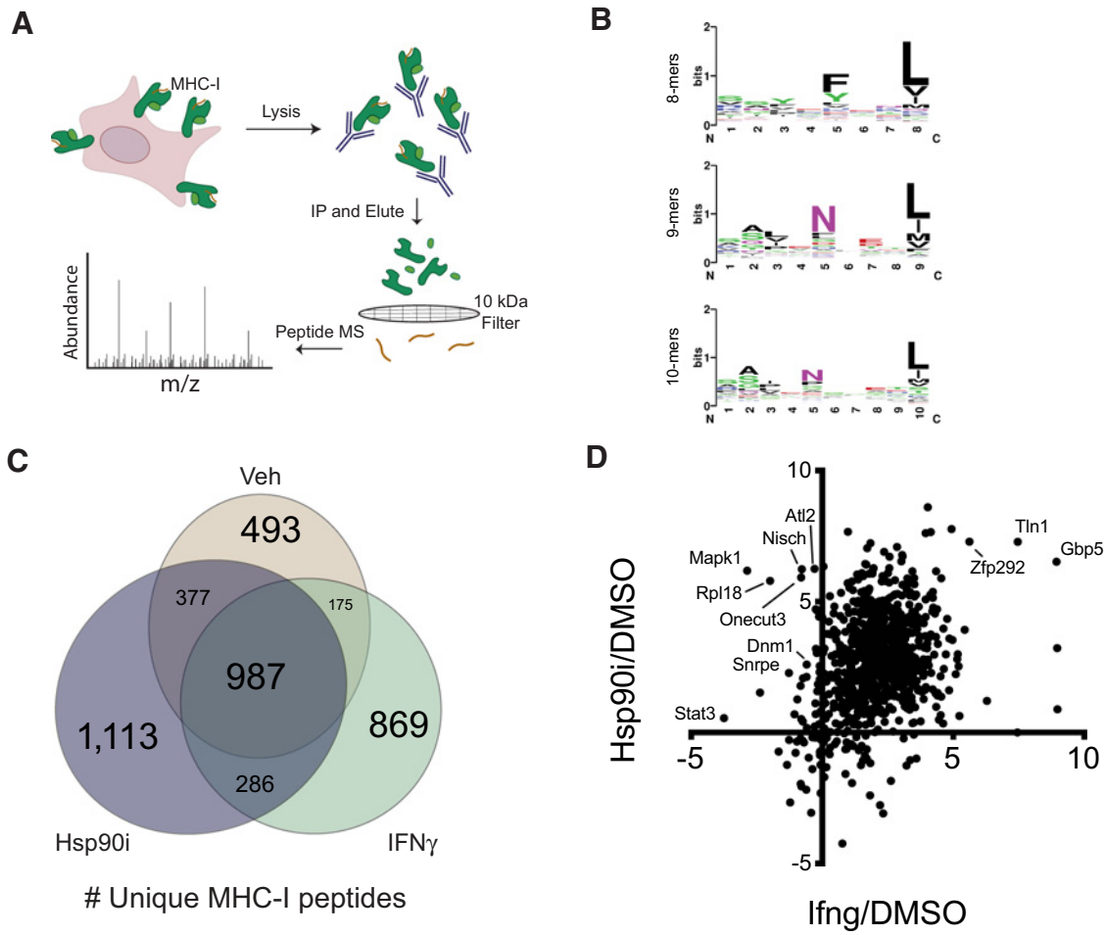

Figure 4.

Hsp90i diversifies the MHC-I antigen repertoire in MC38 cells. **A,** Schematic overview of the protocol for MHC-I peptide profiling. **B,** Amino acid motif analysis of all 8, 9, and 10-mer peptides identified. **C,** Venn diagram of the number of unique MHC-I bound peptides identified in vehicle- (Veh, gold), Hsp90i- treated (purple), and IFNγ-treated (green) samples. The size of each ellipse is proportional to the number of unique peptides identified. **D,** Scatter plot of individual peptides with $\log_2$ fold change IFNγ/DMSO plotted on the *x*-axis and $\log_2$ fold change Hsp90i/DMSO on the *y*-axis. The majority of individual peptides common to both treatment groups are amplified to a similar degree by Hsp90i and IFNγ.

aa), displayed amino acid preferences at known anchor residues for both MHC alleles, and the majority of peptides were predicted to bind H-2K^b and/or H-2D^b with high affinity (Fig. 4B; Supplementary Fig. S4A and S4B). We observed 2,032 unique peptides from vehicle-treated MC38 cells, 2,317 peptides from IFNγ-treated cells, and remarkably, we identified 2,763 unique peptides from Hsp90i-treated cells (Fig. 4C). Notably, more peptides were exclusive to the Hsp90i-treated group (1113) than either Veh (493) or IFNγ (869). Finally, using label-free, semiquantitative analysis for peptides identified in all samples, we observed that both IFNγ and Hsp90i increased the abundance of common MHC-I peptides to a similar degree (Fig. 4D; Supplementary Fig. S4C). Interestingly, some of the peptides present in all samples were more abundant in the Hsp90i-treated samples compared with IFNγ, including peptides derived from Mapk1 and Stat3, which are known to be stabilized by HSP90. Collectively, these results demonstrate that low-level Hsp90i diversifies and amplifies the presentation of a distinct antigen repertoire on tumor cells via a mechanism that is fundamentally distinct from IFNγ signaling.

In vivo efficacy of Hsp90i is dependent on MHC-I

Collectively, our observations led us to a model in which non-heat shock–activating HSP90 inhibition elicits an antitumor immune response by enhancing antigen presentation. Enhancement is mediated through increased expression of immunoproteasome components, presumably generating additional peptides that stabilize surface expression of MHC-I. If correct, this model predicts that deletion of MHC-I from the surface of MC38 cells should ablate the antitumor activity of low-level HSP90 inhibition *in vivo*.

To test the model, we utilized CRISPR/Cas9 to knockout the beta-2 microglobulin gene (*B2m*), causing destabilization of the MHC-I heterocomplex and preventing its trafficking to the cell surface (12). MC38 cells transfected with a control guide RNA (Ctrl) exhibited robust MHC-I surface staining, whereas cells

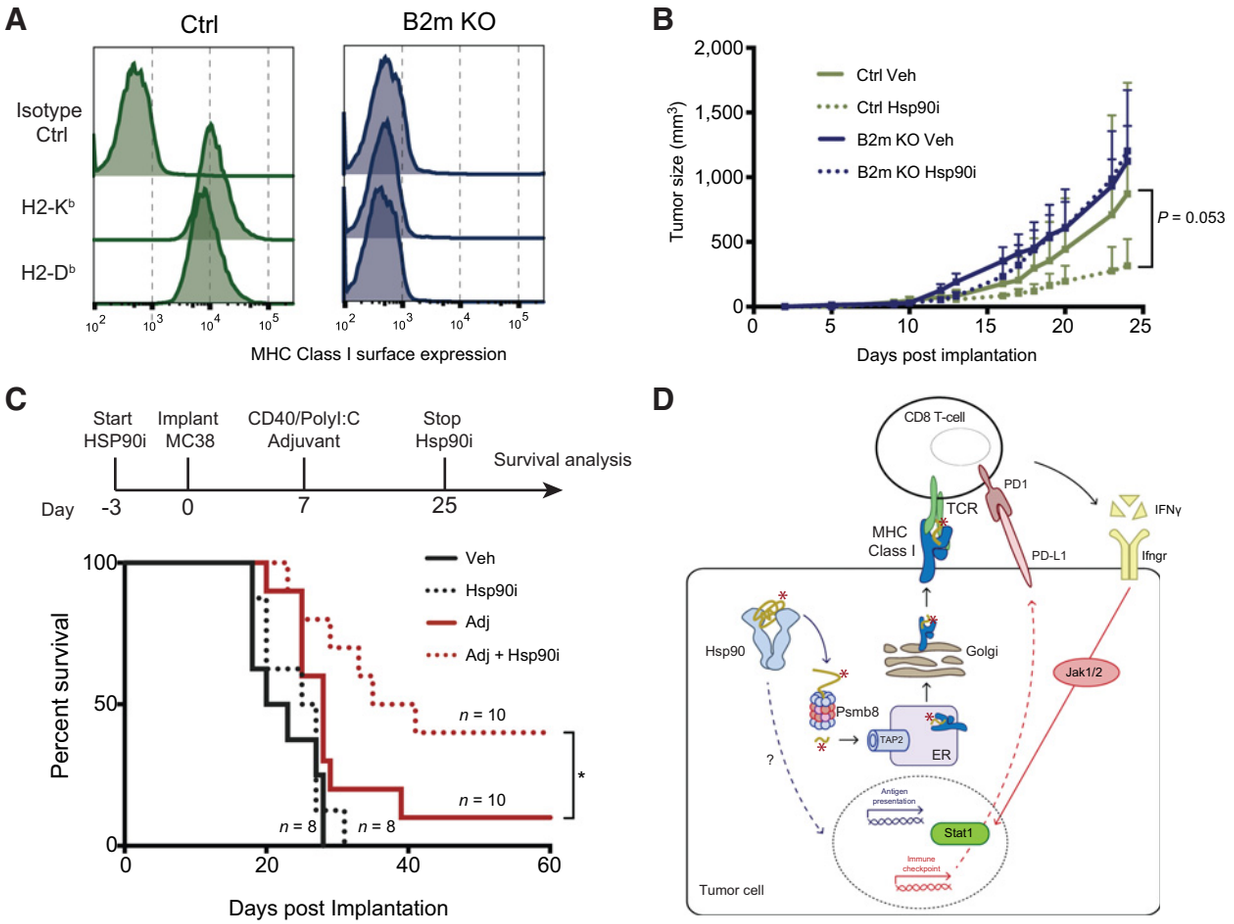

Figure 5.

The antitumor activity of low-dose Hsp90i is dependent on functional MHC-I expression. **A,** Flow cytometric histograms of Ctrl (green) or B2m KO (blue) MC38 cells stained with H2-K^b, H2-D^b, or isotype control antibodies. **B,** Progression of Ctrl (green) or B2m KO (blue) MC38 tumors in mice treated with vehicle (Veh, solid lines) or 0.5 mg/kg/day Hsp90i (dotted lines). **C,** Survival analysis of MC38 tumor-bearing mice treated with vehicle (black, solid line), Hsp90i (black, dotted), CD40/PolyI:C (Adj; red, solid) or Hsp90i + Adj (red, dotted). **D,** Proposed model for HSP90 inhibitor-enhanced antigen presentation and antitumor immunity. Limiting the buffering capacity of HSP90 drives the degradation of mutant, neoantigen-containing proteins (asterisk) via the immunoproteasome and subsequent loading onto MHC-I for presentation in a manner that is distinct from classical IFNγ signaling through Jak/Stat pathways. Increased substrate load clearly plays a causal role, but exactly how Hsp90i-driven flux through the immunoproteasome induces transcriptional upregulation of its subunits and increases cell surface MHC-I level remains to be defined.

transfected with a guide targeting *B2m* (B2m KO) displayed no detectable MHC-I on the cell surface (Fig. 5A).

As expected, the Ctrl and B2m MC38 cells showed no difference in sensitivity to Hsp90i in culture (Supplementary Fig. S5A) and formed tumors, which grew with similar kinetics to that of the parental cells (Fig. 5B, solid lines). Likewise, low-dose Hsp90i treatment reduced the progression of Ctrl tumors to a similar extent as parental MC38 cells, but did not quite reach statistical significance ($P < 0.053$) due to increased variability in the growth of clonally derived CRISPR/Cas9 knock-out cell cultures in mice (Fig. 2A; Fig. 5B). Strikingly, however, MC38 tumors lacking MHC-I (B2m KO) exhibited nearly identical growth kinetics when treated with Hsp90i or vehicle control (Fig. 5B, dotted lines). These results indicate that continuous low-dose administration of Hsp90i elicits an antitumor effect that is at least partially, if not completely dependent on MHC-I expression on the surface of tumor cells.

Hsp90i potentiates the antitumor efficacy of nonspecific immune adjuvant

Finally, we asked whether nonspecific stimulants of the immune system could enhance the ability of Hsp90i treatment to increase antitumor activity. Previous reports using the MC38 syngeneic model have demonstrated that the efficacy of a neoantigen peptide vaccine was potentiated in combination with αCD40/Poly(I:C) adjuvant (36, 38). Administration of agonistic CD40 antibody engages professional antigen-presenting cells (APC) to prime CD8$^+$T cells and in combination with the Toll-like receptor (TLR) ligand Poly(I:C), provides adaptive and innate immune stimulation.

Indeed, treatment of mice carrying MC38 tumors with a combination of continuous low-dose Hsp90i and a single dose of CD40/Poly(I:C) adjuvant cocktail resulted in remarkably increased long-term survival (4/10 mice tumor free after 2 months) compared with either agent alone (Fig. 5C;

Supplementary Fig. S5B). These results indicate that increasing tumor cell antigen presentation through continuous, low-dose Hsp90i exposure can significantly potentiate the antitumor efficacy of conventional nonspecific immunostimulatory interventions.

Discussion

Previous studies have established the capacity of HSP90 to act as a protein-folding buffer that shapes the manifestations of genetic variation in model organisms (22, 23) and in humans (8). Now we show that targeting this fundamental role of HSP90 promotes presentation of the aberrant onco-proteome of cancers to the immune system in the context of MHC-I (Fig. 5D; ref. 39). This approach represents a novel, mechanistically unique way to unmask the "otherness" of highly malignant tumor cells and reveal them to the immune system. By using low, non-heat shock–inducing concentrations of inhibitor, it is possible to rebalance HSP90's role from maintaining the relentlessly anabolic protein metabolism of cancers to favor quality control, proteolytic processing, and antigen presentation (40). From a translational therapeutics perspective, these results suggest a mechanistically unique and pharmacologically tractable method to stimulate specific antitumor immunity.

HSP90 inhibitors were embraced as a new and promising way to simultaneously attack the numerous driver oncoproteins supported by HSP90 and thereby overcome the heterogeneity of clinical cancers that frequently enables the emergence of resistance (10). Unfortunately, clinical testing of an array of highly optimized HSP90 inhibitor chemotypes, either alone or in combination with other agents, has been disappointing. Limited anticancer activity, the most common response being stable disease of variable duration, has prevented any HSP90 inhibitor from advancing to become an approved therapy (41). Given this clinical experience, the problem appears to arise not from the limitations of specific drug scaffolds, but from an underlying flaw in therapeutic rationale.

Sustained inhibition of oncogenic signaling pathways has shown promise in treating tumors harboring driver mutations in kinases (42, 43). In the case of HSP90 inhibitors, toxicity rises markedly as the duration of high-level, client-depleting drug exposure increases. As a result, unlike the daily or more frequent dosing typical of signaling inhibitors, HSP90 inhibitors have been tested in patients almost universally on intermittent, bolus dosing schedules, with drug administered 1–2 times per week (41, 44). Unfortunately, such episodic challenges to protein homeostasis are precisely what the cytoprotective HSR evolved to counteract in guarding the proteome (45). Moreover, activation of Heat Shock Factor 1 (HSF1), the master transcriptional regulator of this response, has recently emerged as a powerful enabler of malignancy, affecting far more than just chaperone levels in both cancer cells and the stromal cells that support them (46, 47).

In addition to activating the HSR, we report that acute, high-dose HSP90 inhibition can impair immune function. However, it is important to acknowledge that patients treated with high doses of HSP90 inhibitors rarely display the classical complications of severely immunosuppressive therapies such as myelosuppression, lymphopenia, or opportunistic infection. While we observed an immunosuppressive gene expression signature following acute HSP90 inhibition, we do not suggest that conventional dosing regimens severely compromise systemic immune function. Rather, we propose that transient, functional impairment of processes such as antigen processing, cytokine production, and T-cell activation resulting from conventional inhibitor dosing schemes may negatively influence antitumor immune responses in the tumor microenvironment. Likely contributing to such an effect, multiple studies have shown that following bolus administration, HSP90 inhibitors are retained at elevated levels in many tumors, long after clearance from the circulation and normal tissues (48, 49). Explanations for this observation remain controversial, but the persistence of suppressive levels of HSP90 inhibitor in the tumor microenvironment, long after clearance from other compartments could profoundly dampen immune mechanisms in the tumor bed. Unfortunately, little or no data addressing these issues are available from the clinical trials that have been done to date.

To avoid HSF1 activation and immunosuppression, yet still limit HSP90 buffering, we employed sustained low-level exposure to an orally bioavailable, moderately potent HSP90 inhibitor that has already undergone clinical testing (44). Using this approach, we achieved rejection of syngeneic tumors in immunocompetent mice at concentrations that are 25- to 50-fold lower than the peak plasma concentrations reported for phase II testing of this drug (continuous 20–40 nmol/L vs. acute ~1,300 nmol/L; ref. 44). In addition to avoiding potentially deleterious immunosuppressive consequences associated with high-dose HSP90 inhibition, such low drug exposures would also be expected to avoid additional dose-limiting toxicities reported in patients such as diarrhea, retinopathy, neurotoxicity, and hepatotoxicity (41, 44).

The mechanism(s) by which low-level HSP90 inhibition enhances MHC-I-associated antigen presentation to stimulate antitumor immune responses remain to be defined completely. Our model suggests that low-dose Hsp90i destabilizes subsets of client proteins, thereby increasing immunoproteasome substrate availability and increasing the abundance of peptides for MHC-I loading. This model stands in contrast to previous reports demonstrating that high-dose HSP90 inhibition limits peptide availability and generates empty MHC-I molecules (13). The importance of peptide abundance is highlighted by rare MHC-I deficiencies caused by mutations in TAP1/2 or tapaisin which result in reduced peptide import into the ER and loading onto MHC-I molecules (50).

On the basis of our transcriptional and MHC-I peptide profiling results, the mechanism(s) we observe also appear clearly distinct from those engaged by classical IFNγ signaling. This finding could have important implications for resistance to immune checkpoint blockade, which can arise following mutational inactivation of IFNγ signaling (2, 34, 35). A recent report describes the induction of a subset of IFN response genes with heat shock–inducing concentrations of HSP90 inhibitor in culture (24). While this report did not directly investigate effects on MHC-I antigen presentation, the results suggest that high level HSP90 inhibition engages IFNγ signaling, whereas our data indicate that low dose stimulates antigen presentation through a distinct mechanism. Thus, low-dose Hsp90i could provide a much needed way to circumvent requirements for IFNγ signaling and stimulate MHC-I surface expression in tumors recurring after checkpoint blockade.

Further work will be required to identify specific tumor-associated antigens that drive the anticancer activity we observed. Are these antigens derived solely from mutated proteins, so called neoantigens? Or does impairing HSP90-mediated buffering and

rebalancing proteostasis drive presentation of antigens derived from certain wild-type proteins, the marked overexpression of which by tumors renders them more dependent on HSP90? While we have not observed physical signs of autoimmune toxicity in our Hsp90i-treated mice, answering these questions will also be helpful in understanding how this treatment paradigm influences immune cell interactions with normal tissues. Assessing the potential for autoimmune toxicity will certainly benefit from using additional preclinical models, including genetically engineered mouse models (GEMM) where the consequences of this treatment paradigm over longer periods of exposure can be more readily assessed. In the clinic, the insights gained could be used to stratify trials by identifying populations most likely to derive benefit. Candidate groups would include patients with cancers in which mismatch repair deficiency or DNA polymerase proofreading mutations results in dramatically increased mutational load or those with EZH2 abnormalities resulting in extensive dysregulation of gene expression (51–53).

A phase Ib trial of the HSP90 inhibitor XL888 and the PD1-inhibitory antibody pembrolizumab is currently enrolling patients with advanced gastrointestinal cancers (NCT03095781). In this trial, the HSP90 inhibitor is being administered on an intermittent schedule at heat shock–inducing doses. Although the trial is not designed to definitively evaluate efficacy, it may provide clues as to whether the immunosuppressive effects of high-level HSP90 inhibition can be counterbalanced by the immunostimulatory effects of a checkpoint antibody.

Although our understanding of HSP90's role in tumor immunology is far from complete, results presented here support the clinical reevaluation of current orally bioavailable HSP90 inhibitors. We propose that therapeutic efficacy for these drugs should be investigated when administered with the intent to enhance tumor immunogenicity while avoiding two therapeutic liabilities—immunosuppression and HSF1 activation. Our results suggest that chronic low-dose Hsp90i is unlikely to produce durable responses as a monotherapy. However, continued investigation of this strategy in additional preclinical models has the potential to identify and the most robust immunomodulatory combinations with the potential for incorporation into clinical trial designs. In performing such trials, pharmacodynamic monitoring of heat shock activation using methods such as reported here could provide a valuable guide to dosing of HSP90 inhibitor. Ironically, heat shock induction has been monitored frequently as a desired pharmacodynamic endpoint in HSP90 inhibitor trials, whereas in the immunoregulatory context, it would serve as a marker of toxicity to be avoided. Indeed, repurposing the extensive development work that has already gone into establishing safety and dosing parameters for such compounds could allow for the very rapid clinical testing of low-dose HSP90 inhibition as a new, mechanistically distinct immunotherapeutic strategy for treating cancers.

Disclosure of Potential Conflicts of Interest

N.U. Lin reports receiving commercial research grants from Synta, Genentech, and Seattle Genetics; reports receiving other commercial research support from Pfizer; is a consultant/advisory board member for Puma and Daichii. A. Jaeger, S. Santagata, L. Whitesell, S. Lindquist, and T. Jacks are listed as co-inventors on a patent application SL 18-02, titled "Combination Treatment of Hsp90 Inhibitors for Enhancing Tumor Immunogenicity and Methods of Use Thereof" to be owned by MIT. No potential conflicts of interest were disclosed by the other authors.

Authors' Contributions

Conception and design: A.M. Jaeger, S. Santagata, N.U. Lin, J.B. Trepel, S. Lindquist, L. Whitesell

Development of methodology: A.M. Jaeger, L. Stopfer, L. Whitesell

Acquisition of data (provided animals, acquired and managed patients, provided facilities, etc.): A.M. Jaeger, L. Stopfer, S. Lee, D. Sandel, N.U. Lin, J.B. Trepel, T. Jacks, L. Whitesell

Analysis and interpretation of data (e.g., statistical analysis, biostatistics, computational analysis): A.M. Jaeger, L. Stopfer, S. Lee, G. Gaglia, N.U. Lin, J.B. Trepel, L. Whitesell

Writing, review, and/or revision of the manuscript: A.M. Jaeger, S. Lee, G. Gaglia, S. Santagata, N.U. Lin, J.B. Trepel, F.M. White, T. Jacks, L. Whitesell

Administrative, technical, or material support (i.e., reporting or organizing data, constructing databases): A.M. Jaeger

Study supervision: F.M. White

Acknowledgments

This work is dedicated to the memory of Susan Lindquist, an insightful scientist and exceptional mentor without whom it could not have been done. We thank Melissa Duquette and Artur Topolski for expert assistance in performing animal experiments and Can Kayatekin, Justin Rettenmaier, and David Canner for helpful discussions. We also thank the Whitehead GTC, especially J. Love, T. Volkert, and S. Gupta for assistance with expression profiling by Nanostring nCounter and RNA sequencing. We thank E. Freinkman and C. Lewis (Whitehead Metabolomics Core) for assistance with drug level monitoring. S. Lindquist was an HHMI investigator. A.M. Jaeger is supported by a postdoctoral fellowship from the Damon Runyon Cancer Research Foundation. L. Stopfer is supported by an MIT Training Grant in Environmental Science. Additional support was provided by Komen Foundation grant KG110450 (to L. Whitesell), the Koch Institute core Grant (NIH P30-CA14051), the Intramural Research Program at the National Cancer Institute (to S. Lindquist and J.B. Trepel), a generous gift from Takeda Pharmaceuticals Immune Oncology Research Fund (to L. Stopfer and F.M. White), and NIH R01 CA194005 (to G. Gaglia and S. Santagata). T. Jacks is an HHMI investigator.

The costs of publication of this article were defrayed in part by the payment of page charges. This article must therefore be hereby marked *advertisement* in accordance with 18 U.S.C. Section 1734 solely to indicate this fact.

Received February 21, 2019; revised April 18, 2019; accepted June 14, 2019; published first June 18, 2019.

References

1. Kandoth C, McLellan MD, Vandin F, Ye K, Niu B, Lu C, et al. Mutational landscape and significance across 12 major cancer types. Nature 2013;502:333–9.
2. Ribas A, Wolchok JD. Cancer immunotherapy using checkpoint blockade. Science 2018;359:1350–5.
3. Sharma P, Allison JP. The future of immune checkpoint therapy. Science 2015;348:56–61.
4. Jenkins RW, Barbie DA, Flaherty KT. Mechanisms of resistance to immune checkpoint inhibitors. Br J Cancer 2018;118:9–16.
5. Sharma P, Hu-Lieskovan S, Wargo JA, Ribas A. Primary, adaptive, and acquired resistance to cancer immunotherapy. Cell 2017;168:707–23.
6. Sade-Feldman M, Jiao YJ, Chen JH, Rooney MS, Barzily-Rokni M, Eliane JP, et al. Resistance to checkpoint blockade therapy through inactivation of antigen presentation. Nat Commun 2017;8:1136.
7. Vartholomaiou E, Echeverria PC, Picard D. Unusual suspects in the twilight zone between the Hsp90 interactome and carcinogenesis. Adv Cancer Res 2016;129:1–30.
8. Karras GI, Yi S, Sahni N, Fischer M, Xie J, Vidal M, et al. HSP90 shapes the consequences of human genetic variation. Cell 2017;168:856–66.
9. Jarosz DF, Lindquist S. Hsp90 and environmental stress transform the adaptive value of natural genetic variation. Science 2010;330:1820–4.

10. Whitesell L, Santagata S, Mendillo ML, Lin NU, Proia DA, Lindquist S. HSP90 empowers evolution of resistance to hormonal therapy in human breast cancer models. Proc Natl Acad Sci U S A 2014;111:18297–302.
11. Tscharke DC, Croft NP, Doherty PC, La Gruta NL. Sizing up the key determinants of the CD8(+) T cell response. Nat Rev Immunol 2015; 15:705–16.
12. Gettinger S, Choi J, Hastings K, Truini A, Datar I, Sowell R, et al. Impaired HLA class I antigen processing and presentation as a mechanism of acquired resistance to immune checkpoint inhibitors in lung cancer. Cancer Discov 2017;7:1420–35.
13. Callahan MK, Garg M, Srivastava PK. Heat-shock protein 90 associates with N-terminal extended peptides and is required for direct and indirect antigen presentation. Proc Natl Acad Sci U S A 2008;105: 1662–7.
14. Cesano A. nCounter((R)) PanCancer Immune Profiling Panel (NanoString Technologies, Inc., Seattle, WA). J Immunother Cancer 2015;3:42.
15. Graner MW. HSP90 and immune modulation in cancer. Adv Cancer Res 2016;129:191–224.
16. Graner MW, Romanoski A, Katsanis E. The `peptidome' of tumour-derived chaperone-rich cell lysate anti-cancer vaccines reveals potential tumour antigens that stimulate tumour immunity. Int J Hyperthermia 2013;29: 380–9.
17. Calderwood SK, Gong J. Molecular chaperones in mammary cancer growth and breast tumor therapy. J Cell Biochem 2012;113:1096–103.
18. Bae J, Mitsiades C, Tai YT, Bertheau R, Shammas M, Batchu RB, et al. Phenotypic and functional effects of heat shock protein 90 inhibition on dendritic cell. J Immunol 2007;178:7730–7.
19. Bae J, Munshi A, Li C, Samur M, Prabhala R, Mitsiades C, et al. Heat shock protein 90 is critical for regulation of phenotype and functional activity of human T lymphocytes and NK cells. J Immunol 2013;190: 1360–71.
20. Taipale M, Jarosz DF, Lindquist S. HSP90 at the hub of protein homeostasis: emerging mechanistic insights. Nat Rev Mol Cell Biol 2010;11: 515–28.
21. Jarosz DF, Taipale M, Lindquist S. Protein homeostasis and the phenotypic manifestation of genetic diversity: principles and mechanisms. Annu Rev Genet 2010;44:189–216.
22. Queitsch C, Sangster TA, Lindquist S. Hsp90 as a capacitor of phenotypic variation. Nature 2002;417:618–24.
23. Rutherford SL, Lindquist S. Hsp90 as a capacitor for morphological evolution. Nature 1998;396:336–42.
24. Mbofung RM, McKenzie JA, Malu S, Zhang M, Peng W, Liu C, et al. HSP90 inhibition enhances cancer immunotherapy by upregulating interferon response genes. Nat Commun 2017;8:451.
25. Proia DA, Kaufmann GF. Targeting heat-shock protein 90 (HSP90) as a complementary strategy to immune checkpoint blockade for cancer therapy. Cancer Immunol Res 2015;3:583–9.
26. Scheper W, Kelderman S, Fanchi LF, Linnemann C, Bendle G, de Rooij MAJ, et al. Low and variable tumor reactivity of the intratumoral TCR repertoire in human cancers. Nat Med 2019;25:89–94.
27. Vigneron N, Van den Eynde BJ. Proteasome subtypes and the processing of tumor antigens: increasing antigenic diversity. Curr Opin Immunol 2012; 24:84–91.
28. Muchamuel T, Basler M, Aujay MA, Suzuki E, Kalim KW, Lauer C, et al. A selective inhibitor of the immunoproteasome subunit LMP7 blocks cytokine production and attenuates progression of experimental arthritis. Nat Med 2009;15:781–7.
29. Gajewski TF, Schreiber H, Fu YX. Innate and adaptive immune cells in the tumor microenvironment. Nat Immunol 2013;14:1014–22.
30. Efremova M, Rieder D, Klepsch V, Charoentong P, Finotello F, Hackl H, et al. Targeting immune checkpoints potentiates immunoediting and changes the dynamics of tumor evolution. Nat Commun 2018;9:32.
31. Benci JL, Xu B, Qiu Y, Wu TJ, Dada H, Twyman-Saint Victor C, et al. Tumor interferon signaling regulates a multigenic resistance program to immune checkpoint blockade. Cell 2016;167:1540–54.
32. Prendergast GC, Mondal A, Dey S, Laury-Kleintop LD, Muller AJ. Inflammatory reprogramming with IDO1 inhibitors: turning immunologically unresponsive `cold' tumors `hot'. Trends Cancer 2018;4:38–58.
33. Gao J, Shi LZ, Zhao H, Chen J, Xiong L, He Q, et al. Loss of IFN-gamma pathway genes in tumor cells as a mechanism of resistance to anti-CTLA-4 therapy. Cell 2016;167:397–404.
34. Wang X, Schoenhals JE, Li A, Valdecanas DR, Ye H, Zang F, et al. Suppression of type I IFN signaling in tumors mediates resistance to anti-PD-1 treatment that can be overcome by radiotherapy. Cancer Res 2017;77: 839–50.
35. Shin DS, Zaretsky JM, Escuin-Ordinas H, Garcia-Diaz A, Hu-Lieskovan S, Kalbasi A, et al. Primary resistance to PD-1 blockade mediated by JAK1/2 mutations. Cancer Discov 2017;7:188–201.
36. Yadav M, Jhunjhunwala S, Phung QT, Lupardus P, Tanguay J, Bumbaca S, et al. Predicting immunogenic tumour mutations by combining mass spectrometry and exome sequencing. Nature 2014;515:572–6.
37. Khodadoust MS, Olsson N, Wagar LE, Haabeth OA, Chen B, Swaminathan K, et al. Antigen presentation profiling reveals recognition of lymphoma immunoglobulin neoantigens. Nature 2017;543:723–7.
38. Llopiz D, Dotor J, Zabaleta A, Lasarte JJ, Prieto J, Borrás-Cuesta F, et al. Combined immunization with adjuvant molecules poly(I:C) and anti-CD40 plus a tumor antigen has potent prophylactic and therapeutic antitumor effects. Cancer Immunol Immunother 2008;57:19–29.
39. Ott PA, Hu Z, Keskin DB, Shukla SA, Sun J, Bozym DJ, et al. An immunogenic personal neoantigen vaccine for patients with melanoma. Nature 2017;547:217–21.
40. Santagata S, Mendillo ML, Tang YC, Subramanian A, Perley CC, Roche SP, et al. Tight coordination of protein translation and HSF1 activation supports the anabolic malignant state. Science 2013;341:1238303.
41. Neckers L, Blagg B, Haystead T, Trepel JB, Whitesell L, Picard D. Methods to validate Hsp90 inhibitor specificity, to identify off-target effects, and to rethink approaches for further clinical development. Cell Stress Chaperones 2018;23:467–82.
42. Motzer RJ, Escudier B, Powles T, Scheffold C, Choueiri TK. Long-term follow-up of overall survival for cabozantinib versus everolimus in advanced renal cell carcinoma. Br J Cancer 2018;118:1176–8.
43. Tate SC, Burke TF, Hartman D, Kulanthaivel P, Beckmann RP, Cronier DM. Optimising the combination dosing strategy of abemaciclib and vemurafenib in BRAF-mutated melanoma xenograft tumours. Br J Cancer 2016; 114:669–79.
44. Spreafico A, Delord JP, De Mattos-Arruda L, Berge Y, Rodon J, Cottura E, et al. A first-in-human phase I, dose-escalation, multicentre study of HSP990 administered orally in adult patients with advanced solid malignancies. Br J Cancer 2015;112:650–9.
45. McMillan DR, Xiao X, Shao L, Graves K, Benjamin IJ. Targeted disruption of heat shock transcription factor 1 abolishes thermotolerance and protection against heat-inducible apoptosis. J Biol Chem 1998;273: 7523–8.
46. Dai C, Whitesell L, Rogers AB, Lindquist S. Heat shock factor 1 is a powerful multifaceted modifier of carcinogenesis. Cell 2007;130:1005–18.
47. Scherz-Shouval R, Santagata S, Mendillo ML, Sholl LM, Ben-Aharon I, Beck AH, et al. The reprogramming of tumor stroma by HSF1 is a potent enabler of malignancy. Cell 2014;158:564–78.
48. Graham B, Curry J, Smyth T, Fazal L, Feltell R, Harada I, et al. The heat shock protein 90 inhibitor, AT13387, displays a long duration of action in vitro and in vivo in non-small cell lung cancer. Cancer Sci 2012;103: 522–7.
49. Shimamura T, Perera SA, Foley KP, Sang J, Rodig SJ, Inoue T, et al. Ganetespib (STA-9090), a nongeldanamycin HSP90 inhibitor, has potent antitumor activity in in vitro and in vivo models of non-small cell lung cancer. Clin Cancer Res 2012;18:4973–85.
50. Hanna S, Etzioni A. MHC class I and II deficiencies. J Allergy Clin Immunol 2014;134:269–75.
51. Le DT, Durham JN, Smith KN, Wang H, Bartlett BR, Aulakh LK, et al. Mismatch repair deficiency predicts response of solid tumors to PD-1 blockade. Science 2017;357:409–13.
52. Bourdais R, Rousseau B, Pujals A, Boussion H, Joly C, Guillemin A, et al. Polymerase proofreading domain mutations: new opportunities for immunotherapy in hypermutated colorectal cancer beyond MMR deficiency. Crit Rev Oncol Hematol 2017;113:242–8.
53. Kim KH, Roberts CW. Targeting EZH2 in cancer. Nat Med 2016;22:128–34.